Improved Estimators of Faraday Rotation in Spaceborne Polarimetric SAR Data

Jie Chen, *Member, IEEE*, and Shaun Quegan, *Member, IEEE*

***Abstract*—Spaceborne polarimetric synthetic aperture radar systems operating at lower frequencies, such as P-band, are significantly affected by Faraday rotation (FR). A new set of FR estimators is derived from the off-diagonal terms in the measured covariance matrix of a distributed target. These estimators have a phase ambiguity of period π, instead of $\pi/2$ as for the published estimators, and this ambiguity can be completely resolved for arbitrarily large values of FR using total electron content maps derived from Global Navigation Satellite System measurements. Simulations show that one of the new estimators has particularly high resistance to system noise and channel amplitude imbalance but greater sensitivity to channel phase imbalance than the published estimators. Hence, the expected values of residual system distortion after calibration may affect the choice of estimator.**

***Index Terms*—Biomass, Faraday rotation (FR), ionospheric effects, polarimetry, synthetic aperture radar (SAR).**

I. Introduction

THE SUCCESSFUL deployment of the Phased Array L-band Synthetic Aperture Radar (PALSAR) in orbit in January 2006 marks the start of sustained observation of the Earth by lower frequency spaceborne SARs. L-band SAR missions are planned by several space agencies, and the European Space Agency is currently conducting Phase-A studies for the P-band BIOMASS mission, which will measure global forest biomass. However, the ionosphere can significantly affect such systems; in particular, L- and P-band spaceborne SAR measurements will suffer from Faraday rotation (FR) [1]–[3], whose one-way value has been estimated to be as large as 40° at L-band and 320° at P-band [4], [5] at solar maximum. Several FR estimators have been suggested [5]–[8], but they all suffer from a $\pm k\pi/2$ ambiguity, which is a particular problem at P-band. To deal with this, a method similar to phase unwrapping has been designed, assuming gradual spatial change in FR [8], but it is difficult to fix a benchmark of zero FR to start this process.

This letter proposes a new method for FR correction based on analysis of the measured covariance matrix of polarimetric SAR data. After an introduction to the existing FR estimators in Section II, a set of improved FR estimators with $\pm k\pi$ ambiguity is proposed in Section III. It is demonstrated that this ambiguity can be removed by using global total electron content (TEC) maps provided by the Global Navigation Satellite System (GNSS). Both the polarimetric scattering vector and the covariance matrix can then be correctly retrieved from the measured data. The computer simulations and analysis presented in Section IV verify the effectiveness of the approach.

Manuscript received August 7, 2009; revised November 24, 2009 and February 18, 2010. Date of publication June 10, 2010; date of current version October 13, 2010. This work was supported in part by the National Natural Science Foundation of China under Grant 60602045 and in part by the New Century Excellent Talent Program of the Chinese Ministry of Education under Grant NCET-06-0166.

J. Chen was with the School of Mathematics and Statistics, University of Sheffield, Sheffield, S3 7RH, U.K. He is now with the School of Electronic and Information Engineering, Beihang University (BUAA), Beijing 100191, China (e-mail: chenjie@buaa.edu.cn).

S. Quegan is with the School of Mathematics and Statistics, University of Sheffield, S3 7RH Sheffield, U.K. (e-mail: s.quegan@sheffield.ac.uk).

Digital Object Identifier 10.1109/LGRS.2010.2047002

II. Estimation of Faraday Rotation

A. Faraday Rotation

When a polarized electromagnetic wave traverses the ionosphere, its interaction with free electrons and the Earth's magnetic field leads to rotation of the polarization vector [9]–[12]. This phenomenon is known as Faraday rotation. The one-way Faraday rotation for a SAR signal can be approximated as [12]

$$\Omega = \frac{K}{f_0^2} \cdot \overline{B\cos\psi \cdot \sec\theta} \cdot TEC \tag{1}$$

where f_0 is the carrier frequency in hertz, K is a constant of value 2.365×10^4 $[\mathrm{A}\cdot\mathrm{m}^2/\mathrm{kg}]$, B is the magnetic flux density in webers per square meter, and ψ and θ are the angles that the wave normal makes with the Earth's magnetic field and the downward vertical, respectively. TEC is in TEC units (1 TECU $= 10^{16}$ electrons $\cdot\,\mathrm{m}^{-2}$). The magnetic field factor $(\overline{B\cos\psi\cdot\sec\theta})$ is calculated at a height of 400 km.

The measured scattering matrix $\mathbf{M}$ with FR and system errors (channel imbalance, crosstalk, and noise) can be written as [6]

$$\begin{aligned}\mathbf{M} &= \begin{bmatrix} M_{\mathrm{hh}} & M_{\mathrm{vh}} \\ M_{\mathrm{hv}} & M_{\mathrm{vv}} \end{bmatrix} \\ &= A(r,\theta)e^{j\varphi} \begin{bmatrix} 1 & \delta_2 \\ \delta_1 & f_1 \end{bmatrix} \cdot \begin{bmatrix} \cos\Omega & \sin\Omega \\ -\sin\Omega & \cos\Omega \end{bmatrix} \\ &\quad \cdot \begin{bmatrix} S_{\mathrm{hh}} & S_{\mathrm{vh}} \\ S_{\mathrm{hv}} & S_{\mathrm{vv}} \end{bmatrix} \cdot \begin{bmatrix} \cos\Omega & \sin\Omega \\ -\sin\Omega & \cos\Omega \end{bmatrix} \cdot \begin{bmatrix} 1 & \delta_3 \\ \delta_4 & f_2 \end{bmatrix} \\ &\quad + \begin{bmatrix} N_1 & N_3 \\ N_2 & N_4 \end{bmatrix} \end{aligned} \tag{2}$$

where S_{hh}, S_{hv}, S_{vh}, and S_{vv} are the components of the true scattering matrix (assumed to be reciprocal, i.e., $S_{\mathrm{hv}} = S_{\mathrm{vh}}$); f_1 and f_2 denote channel imbalance terms; δ_i, $i = 1{-}4$, are radar crosstalk terms; and N_i, $i = 1{-}4$, are additive noise terms present in each measurement. This letter deals primarily with estimation of and correction for FR when system effects are negligible or have been corrected (using methods such as those described in [5]), but the effects of system noise and residual channel imbalance on FR correction methods are also considered.

B. FR Angle Estimators

Bickel and Bates [7] proposed the first FR estimator

$$\hat{\Omega} = \frac{1}{4}\arg\left(Z_{21}Z_{12}^{*}\right) \tag{3}$$

where $Z_{12} = (M_{\rm hv} - M_{\rm vh}) + j(M_{\rm hh} + M_{\rm vv})$ and $Z_{21} = Z_{12} + 2(M_{\rm vh} - M_{\rm hv})$.

Under the assumption of azimuthal reflection symmetry, i.e., $\langle S_{\rm hh}\ S_{\rm hv}^{*}\rangle = \langle S_{\rm vv}\ S_{\rm hv}^{*}\rangle = 0$, Freeman [5] proposed two FR estimators. The first is given by

$$\hat{\Omega} = \frac{1}{2}\tan^{-1}\left[\frac{M_{\rm vh} - M_{\rm hv}}{M_{\rm hh} + M_{\rm vv}}\right]. \tag{4}$$

We do not include this in our analysis because, as pointed out in [5] and [9], this pixel-based method is prone to large errors (not only does it involve the ratio of two zero-mean complex numbers, but also the argument of the $\tan^{-1}$ function may be complex in the presence of noise). These problems can be removed by using average quantities, as proposed in Freeman's second estimator

$$\hat{\Omega} = \pm\frac{1}{2}\tan^{-1}\sqrt{\frac{\langle|M_{\rm hv} - M_{\rm vh}|^2\rangle}{\langle|M_{\rm hh} + M_{\rm vv}|^2\rangle}}. \tag{5}$$

Qi and Jin [8] also presented an FR estimator given by

$$\hat{\Omega} = -\frac{1}{2}\tan^{-1}\left[\frac{\mathrm{Im}\,\langle M_{\rm hh}\,(M_{\rm hv}^{*} - M_{\rm vh}^{*})\rangle}{\mathrm{Im}\,\langle M_{\rm hh}M_{\rm vv}^{*}\rangle}\right]. \tag{6}$$

Note that [8] contains a sign error, which is corrected in (6). All these estimators give a value of FR in the range of $\pm\pi/4$, so they have an ambiguity error of $\pm k\pi/2$, where k is an integer.

III. New Set of FR Estimators

A. Analysis of Covariance Matrix Elements

The covariance matrix of the true scattering vector can be written as

$$\mathbf{C_S} = \langle \mathbf{S}\cdot\mathbf{S}^{+}\rangle = \begin{bmatrix} \sigma_1 & \rho_{12} & \rho_{13} \\ \rho_{21} & \sigma_2 & \rho_{23} \\ \rho_{31} & \rho_{32} & \sigma_3 \end{bmatrix} \tag{7}$$

where $\mathbf{S} = [S_{\rm hh}, S_{\rm hv}, S_{\rm vv}]^{\rm t} \equiv [S_1, S_2, S_3]^{\rm t}$ is the true scattering vector, $\sigma_p = \langle S_p\ S_p^{*}\rangle$ is the backscattered power in the pth channel, and $\rho_{pq} = \langle S_p\ S_q^{*}\rangle$ is the covariance of channels p and q, where p and q take the values of 1, 2, or 3.

From (2), if FR is the only error source in the signal, the measured scattering matrix has terms [5]

$$\begin{aligned} M_{\rm hh} &\equiv M_1 = S_{\rm hh}\cos^2\Omega - S_{\rm vv}\sin^2\Omega \\ M_{\rm hv} &\equiv M_2 = S_{\rm hv} - (S_{\rm hh} + S_{\rm vv})\sin\Omega\cos\Omega \\ M_{\rm vh} &\equiv M_3 = S_{\rm hv} + (S_{\rm hh} + S_{\rm vv})\sin\Omega\cos\Omega \\ M_{\rm vv} &\equiv M_4 = -S_{\rm hh}\sin^2\Omega + S_{\rm vv}\cos^2\Omega \end{aligned} \tag{8}$$

so that $M_{\rm hv} \neq M_{\rm vh}$. Note that these expressions all have period π in terms of Ω.

The covariance matrix of the measured scattering vector can then be written as the 4×4 matrix $\mathbf{C}$, where $C_{pq} = \langle M_p\ M_q^{*}\rangle$ is the covariance of channels p and q, and p and q take the values of 1, 2, 3, or 4. It is readily shown that the imaginary parts of the off-diagonal terms in $\mathbf{C}$ can be written as

$$\begin{cases} \mathrm{Im}(C_{12}) = \mathrm{Im}(\rho_{12}\cos^2\Omega - \rho_{13}\sin\Omega\cos\Omega + \rho_{23}\sin^2\Omega) \\ \mathrm{Im}(C_{13}) = \mathrm{Im}(\rho_{12}\cos^2\Omega + \rho_{13}\sin\Omega\cos\Omega + \rho_{23}\sin^2\Omega) \\ \mathrm{Im}(C_{14}) = \mathrm{Im}(\rho_{13})\cos 2\Omega \\ \mathrm{Im}(C_{23}) = -\mathrm{Im}(\rho_{12} - \rho_{23})\sin 2\Omega \\ \mathrm{Im}(C_{24}) = \mathrm{Im}(\rho_{23}\cos^2\Omega - \rho_{13}\sin\Omega\cos\Omega + \rho_{12}\sin^2\Omega) \\ \mathrm{Im}(C_{34}) = \mathrm{Im}(\rho_{23}\cos^2\Omega + \rho_{13}\sin\Omega\cos\Omega + \rho_{12}\sin^2\Omega). \end{cases} \tag{9}$$

From (9), we can derive the following two sets of equations:

$$\mathrm{Im}(\rho_{13})\cos 2\Omega = \mathrm{Im}(C_{14}) \tag{10}$$

$$\begin{cases} \mathrm{Im}(\rho_{13})\sin 2\Omega = \mathrm{Im}(C_{13} - C_{12}) \\ \mathrm{Im}(\rho_{13})\sin 2\Omega = \mathrm{Im}(C_{34} - C_{24}) \\ \mathrm{Im}(\rho_{13})\sin 2\Omega = \mathrm{Im}(C_{13} + C_{34} - C_{12} - C_{24})/2 \end{cases} \tag{11}$$

$$\mathrm{Im}(\rho_{12} - \rho_{23})\sin 2\Omega = -\mathrm{Im}(C_{23}) \tag{12}$$

$$\begin{cases} \mathrm{Im}(\rho_{12} - \rho_{23})\cos 2\Omega = \mathrm{Im}(C_{12} - C_{24}) \\ \mathrm{Im}(\rho_{12} - \rho_{23})\cos 2\Omega = \mathrm{Im}(C_{13} - C_{34}) \\ \mathrm{Im}(\rho_{12} - \rho_{23})\cos 2\Omega = \mathrm{Im}(C_{12} + C_{13} - C_{24} - C_{34})/2. \end{cases} \tag{13}$$

From (10)–(13), we can construct three expressions for $\mathrm{Im}(\rho_{13})e^{2j\Omega}$, denoted by Z_i, $i = 1$–3, and three expressions for $[\mathrm{Im}(\rho_{12}) - \mathrm{Im}(\rho_{23})]e^{2j\Omega}$, denoted by Z_i, $i = 4$–6, namely

$$\begin{cases} Z_1 = \mathrm{Im}(C_{14}) + j\mathrm{Im}(C_{13} - C_{12}) \\ Z_2 = \mathrm{Im}(C_{14}) + j\mathrm{Im}(C_{34} - C_{24}) \\ Z_3 = \mathrm{Im}(C_{14}) + j\mathrm{Im}(C_{13} + C_{34} - C_{12} - C_{24})/2 \\ Z_4 = \mathrm{Im}(C_{12} - C_{24}) - j\mathrm{Im}(C_{23}) \\ Z_5 = \mathrm{Im}(C_{13} - C_{34}) - j\mathrm{Im}(C_{23}) \\ Z_6 = \mathrm{Im}(C_{12} - C_{24} + C_{13} - C_{34})/2 - j\mathrm{Im}(C_{23}). \end{cases} \tag{14}$$

B. Estimation of FR With Complex Statistics

Each of the complex quantities Z_i in (14) provides an estimate of FR given by

$$\widehat{\Omega}_i = \frac{1}{2}\arg\{Z_i\}, \qquad i = 1 - 6. \tag{15}$$

These estimates of FR lie between $\pm\pi/2$, whereas the published estimators outlined in Section II lie between $\pm\pi/4$.

For $i = 1{-}3$

$$\begin{aligned} \widehat{\Omega}_i &= \frac{1}{2}\arg\left\{\mathrm{Im}(\rho_{13})e^{2j\Omega}\right\} \\ &= \begin{cases} \Omega - \frac{\pi}{2} \pm k\pi, & \text{if } \mathrm{Im}(\rho_{13}) < 0 \\ \Omega \pm k\pi, & \text{if } \mathrm{Im}(\rho_{13}) \geq 0 \end{cases} \end{aligned} \tag{16}$$

where k is an integer.

Similarly, for $i = 4{-}6$

$$\begin{aligned} \widehat{\Omega}_i &= \frac{1}{2}\arg\left\{[\mathrm{Im}(\rho_{12} - \rho_{23})]\,e^{2j\Omega}\right\} \\ &= \begin{cases} \Omega - \frac{\pi}{2} \pm k\pi, & \text{if } \mathrm{Im}(\rho_{12}) < \mathrm{Im}(\rho_{23}) \\ \Omega \pm k\pi, & \text{if } \mathrm{Im}(\rho_{12}) \geq \mathrm{Im}(\rho_{23}) \end{cases} \end{aligned} \tag{17}$$

TABLE I
FR ERROR AT P-BAND AS A FUNCTION OF LATITUDE FOR A TEC ERROR OF 10 TECU AND A CENTERED DIPOLE MAGNETIC FIELD

Latitude (degrees)	FR error (degrees)
0	1.30
20	13.5
40	24.4
60	32.4
80	36.6

The formulas (16) and (17) all contain a phase ambiguity of $\pm k\pi$, which is irrelevant for polarimetric SAR analysis but may be significant for polarimetric interferometry [5], [13]. However, if $\mathrm{Im}(\rho_{13}) < 0$ or $\mathrm{Im}(\rho_{12}) < \mathrm{Im}(\rho_{23})$, the $-\pi/2$ phase error in (16) and (17) will cause errors in correcting FR in polarimetric SAR data.

C. Ambiguity Error Correction Using TEC Data

Both types of phase error can be removed by using (1) to provide an independent prediction of FR, where TEC is given by the global ionospheric TEC maps estimated by GNSS and use is made of the IGRF10 model for the Earth's magnetic field [1], [10], [11]. The International GNSS Service provides bihourly global TEC maps with grid points spaced 5° in longitude and 2.5° in latitude [10], [11], [14]. Comparison of global TEC maps derived from GPS data with very long baseline interferometry observations and independent TOPEX/JASON observations indicated overall root-mean-square (rms) differences of 3–5 TECU [14], [15]. The corresponding FR errors can be estimated using the simplified formula presented in [12] ((5), and (6)) for a centered dipole magnetic field

$$\Omega = 0.339 \times \frac{TECU}{f_0^2} \times (2\sin\Phi \pm \cos\lambda \cdot \tan\theta_0) \qquad (18)$$

where Ω is given in degrees, f_0 is in gigahertz, Φ is the latitude, λ is the orbit inclination, and θ_0 is the radar elevation angle. The $\pm$ sign indicates right- or left-looking. For a P-band system operating at 435 MHz with $\lambda = 80^\circ$ and $\theta_0 = 23^\circ$, an error of 10 TECU therefore yields FR errors which depend on latitude Φ, as shown in Table I.

Hence, an FR estimator correcting for both types of phase error is given by

$$\widehat{\Omega}_i^F = \widehat{\Omega}_i + \mathrm{round}\left(\frac{\widehat{\Omega}_{GNSS} - \widehat{\Omega}_i}{\pi/2}\right) \cdot \frac{\pi}{2}, \qquad i = 1 - 6 \qquad (19)$$

where round$\{\cdot\}$ denotes rounding to the nearest integer, $\widehat{\Omega}_{\mathrm{GNSS}}$ is the FR predicted from GNSS TEC data, and $\widehat{\Omega}_i$ is taken from (15). A similar approach can be applied to the published FR estimators (3), (5), and (6) described in Section II, although this will not resolve the sign ambiguity in (5) near multiples of π, and errors will be larger for such values of FR. However, the new estimators can tolerate larger errors in the TEC data because they have an ambiguity of π rather than $\pi/2$. In the noise-free case, this will only confer an advantage for unusually large errors in the GPS-derived maps, even at high latitudes (see Table I), but makes the new estimators more noise resistant, as discussed in Section IV-B.

In order to improve the accuracy of the estimates, we use a subimage of 100 × 100 pixels divided into 400 individual windows of 5 × 5 pixels. The covariance matrix and the associated FR are estimated for each window, and the mean of the 400 estimated FR values gives the final estimate $\widehat{\Omega}_i^F$. For the Bickel and Bates estimator, it is instead estimated by averaging the pixel-based estimates of FR over the whole subimage [9], [10].

D. Sensitivity to System Noise

In exact calculations, any of the estimators in (15) might be considered suitable for estimating FR. However, $\hat{\Omega}_4^F$, $\hat{\Omega}_5^F$, and $\widehat{\Omega}_6^F$ depend on the off-diagonal terms of the true covariance matrix [see (12) and (13)], so they would be identically zero under reflection symmetry. In addition, all the estimators are affected by system noise. If the noise in different channels is uncorrelated, i.e., $\langle N_p\ N_q^* \rangle = 0$ if $p \neq q$, and is also uncorrelated with the signal, i.e., $\langle M_p\ N_q^* \rangle = 0$ for all p and q, then, for $p \neq q$

$$C'_{pq} = \left\langle (M_p + N_p)\left(M_q^* + N_q^*\right)\right\rangle = \left\langle M_p M_q^* \right\rangle = C_{pq} \qquad (20)$$

where C_{pq} is the noise-free covariance. Hence, the real and imaginary parts of the complex statistics Z_i in (14) will be unbiased. Furthermore, the simulations in Section IV illustrate that the estimators are stable even if the signal-to-noise ratio (SNR), defined as

$$SNR = \frac{\sigma_1 + 2\sigma_2 + \sigma_3}{\sum_{i=1}^{4} \langle |N_i|^2 \rangle} \qquad (21)$$

is as low as 0 dB.

IV. SIMULATION RESULTS AND DISCUSSION

A. Simulation Parameters

Single-look complex P-band data from the National Aeronautics and Space Administration Jet Propulsion Laboratory AIRSAR system over the agricultural region of Feltwell, U.K., were utilized to simulate FR effects on a spaceborne polarimetric P-band SAR. These SAR images were subsampled to remove spatial correlation and make pixels effectively independent, and then corrupted by FR with values ranging from -180° to 180° in steps of 1°. For each value of FR, simulated complex white Gaussian noise was added to each channel. The noise power was the same in each channel, and the SNR was varied from 0 to 50 dB.

In order to simulate the impact of GNSS TEC errors on estimator performance, we assumed an unbiased Gaussian TEC error with a standard deviation (SD) of 5 TECU; since the TEC error is linearly related to the FR error, this corresponds to an FR error with an SD of 13° at latitude $\Phi = 40^\circ$ (see (18) and Table I). The data were then amalgamated for all values of FR, so the performance measures depend only on SNR.

B. Simulation of FR Estimation Performance

The simulations show that the use of $\widehat{\Omega}_{\mathrm{GNSS}}$ data ensures that the new estimators are all unbiased, even when the FR values are extended over the range of -360° to 360°. However, the

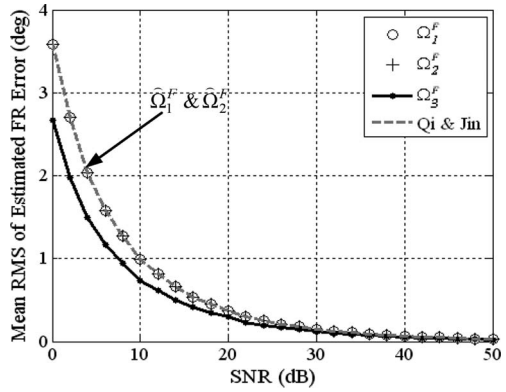

Fig. 1. Simulated noise sensitivity of $\widehat{\Omega}_1^F$–$\widehat{\Omega}_3^F$ and the Qi and Jin estimator.

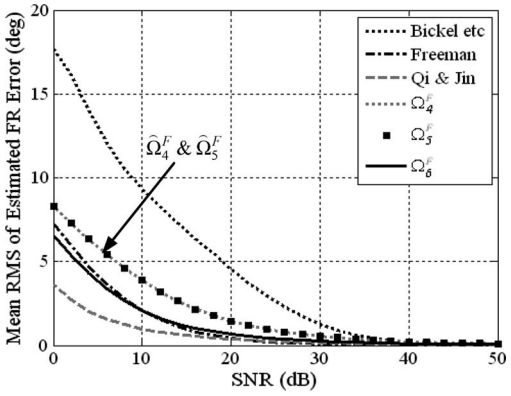

Fig. 2. Simulated noise sensitivity of $\widehat{\Omega}_4^F$–$\widehat{\Omega}_6^F$ and the published estimators.

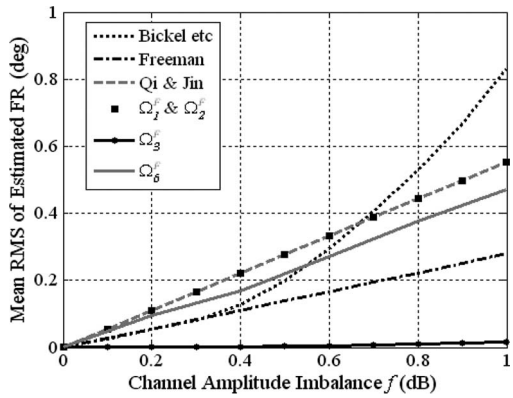

Fig. 3. Mean rms error in FR as a function of channel amplitude imbalance for the different FR estimators ($f_1 = f_2 = f$; $\Delta\phi = 0°$; $\langle |N_i|^2 \rangle = 0, i = 1{-}4$).

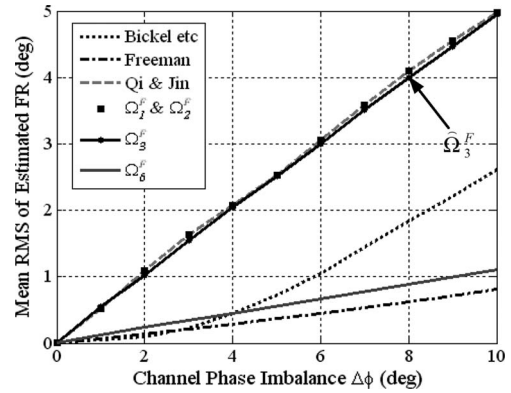

Fig. 4. Mean rms error in FR as a function of channel phase imbalance for the FR estimators ($\arg\{f_1\} = \arg\{f_2\} = \Delta\phi$; $|f_1| = |f_2| = 1$; $\langle |N_i|^2 \rangle = 0, i = 1{-}4$).

rms of the estimated FR error, evaluated in the range of $\pm 180°$ in steps of $1°$, exposes differences in estimator performance. The mean rms error was estimated by averaging the rms errors measured within 80 randomly selected 100×100 pixel areas in the AIRSAR data set. Figs. 1 and 2 show its value (in degrees) as a function of SNR for the new FR estimators (19) and the published FR estimators (note the different scales on the y-axes in Figs. 1 and 2, and that $\widehat{\Omega}_1^F \cong \widehat{\Omega}_2^F$ and $\widehat{\Omega}_4^F \cong \widehat{\Omega}_5^F$).

Fig. 1 shows the robustness of estimators $\widehat{\Omega}_1^F$–$\widehat{\Omega}_3^F$. Even for an SNR as low as 0 dB, the rms error for $\widehat{\Omega}_3^F$ is less than $3°$ (if there were no GNSS TEC errors, the corresponding rms error would be less than $0.8°$). Fig. 1 also shows that the Qi and Jin estimator gives comparable performance to $\widehat{\Omega}_1^F$ and $\widehat{\Omega}_2^F$, while $\widehat{\Omega}_3^F$ performs slightly better. Fig. 2 shows that the other estimators perform less well. In particular, $\widehat{\Omega}_4^F$–$\widehat{\Omega}_6^F$ are sensitive to noise because the AIRSAR data were acquired from an agricultural region where azimuthal reflection symmetry is likely to hold, so that ρ_{12} and ρ_{23} have small values [see (12) and (13)]. The Bickel and Bates estimator has the worst performance because the estimation error increases greatly when Ω is near $\pm(2k+1)\pi/4$. For the Freeman estimator, the estimation error rises when Ω is near $\pm k\pi/4$ (it is important to note that this includes $0°$).

C. Simulation of Channel Imbalance Effects

The previous analysis does not account for system errors such as channel imbalance and crosstalk, but the various FR estimators have different tolerance to such errors. Here, we only present a simplified analysis in which we assume that crosstalk has been corrected using a procedure such as that described in [5], but a residual channel imbalance still remains. We further assume a reciprocal system with the same channel imbalance on transmit and receive ($f_1 = f_2 = f$ in (2)) and neglect system noise. Channel imbalance effects were simulated with FR varying from $-180°$ to $180°$ in steps of $1°$ and for two cases: 1) Phase imbalance was set to $0°$, and amplitude imbalance was varied from 0 to 1 dB, and 2) amplitude imbalance was set to 0 dB, and phase imbalance $\arg\{f_1\} = \arg\{f_2\} = \Delta\phi$ was varied from $0°$ to $10°$.

For a given channel imbalance, the error in the estimated FR depends on FR, so, in Figs. 3 and 4, we show the rms error for $\widehat{\Omega}_1^F$ to $\widehat{\Omega}_3^F$ and the published estimators across the full range of FR angles for cases 1) and 2), respectively. Note that $\widehat{\Omega}_1^F$ and $\widehat{\Omega}_2^F$ exhibit the same performance. The highest tolerance to amplitude imbalance is exhibited by $\widehat{\Omega}_3^F$, although the rms errors are quite small for all of them. Fig. 4 shows that the rms error for all the estimators, except for the Bickel and Bates estimator, depends nearly linearly on phase imbalance, and that the new estimators $\widehat{\Omega}_1^F$–$\widehat{\Omega}_3^F$, together with the Qi and Jin estimator, have the greatest sensitivity to this form of distortion (and, for reasons that are yet unknown, significantly more sensitivity than $\widehat{\Omega}_6^F$). The Freeman estimator exhibits only a slight dependence on phase imbalance, and overall, this estimator appears to be most robust to channel imbalance.

TABLE II
PREDICTED AND ESTIMATED FR FOR THE ALOS/PALSAR DATA SET

Image area	TEC_{GNSS} (TECU)	$\widehat{\Omega}_{GNSS}$ (deg)	$\widehat{\Omega}_{Beckel}$ (deg)	$\widehat{\Omega}_{Freeman}$ (deg)	$\widehat{\Omega}_{Qi\ \&\ Jin}$ (deg)	$\widehat{\Omega}_3^F$ (deg)	$\widehat{\Omega}_6^F$ (deg)
Indonesia	6.59	-0.556	-0.4234	-3.5456	-0.3238	-0.4236	-0.3938
Germany	6.58	2.001	1.0374	3.3179	0.9504	0.9798	0.9369

D. Evaluation of FR Estimators With ALOS PALSAR Data

The new FR estimators were tested on two ALOS PALSAR full-pol data sets, i.e., one from an area in Indonesia acquired on May 13, 2009, and one from Germany acquired on February 2, 2007. The FR predicted using GNSS TEC data and the mean FR estimated with different estimators are listed in Table II. The $\widehat{\Omega}_3^F$, $\widehat{\Omega}_6^F$, and Qi and Jin estimators have nearly the same performance as the Bickel and Bates estimator, suggesting that the new estimators perform correctly, since, for an FR near 0°, simulations (not shown) indicate that the Bickel and Bates estimator is much less affected by noise than the Freeman estimator, while Figs. 3 and 4 show its resistance to small system errors.

E. Discussion

A useful context for assessing these results is the proposed European Space Agency P-band BIOMASS mission, for which the noise equivalent σ° (NESZ) is specified to lie within -25 and -30 dB for fully polarimetric (i.e., single-look) data [16]. Over forest regions, the P-band backscattering coefficients have values around -16 to -9 dB and -17 to -11 dB for HH and VV, respectively, and -25 to -15 dB for HV [17]. As a result, the SNR lies in the range of 10–20 dB for forest regions. Figs. 1 and 2 show that, over this range, the $\widehat{\Omega}_1^F$, $\widehat{\Omega}_2^F$, $\widehat{\Omega}_3^F$ and Qi and Jin estimators perform much better than the others considered, with $\widehat{\Omega}_3^F$ giving the best performance.

The proposed limits on channel imbalance for the BIOMASS mission are that its amplitude must be less than 1 dB and its phase must not exceed 5°–10° [18]. Figs. 3 and 4 show that $\widehat{\Omega}_3^F$ is insensitive to channel amplitude imbalance, but that phase imbalance significantly reduces its performance. However, in [11], it was found that the residual phase imbalance in the calibrated ALOS PALSAR data has a mean value of less than 0.88° and an SD of about 0.45°. Comparable accuracy in calibrating the BIOMASS P-band radar will yield rms FR errors of around 0.5° for $\widehat{\Omega}_3^F$ and only 0.2° for $\widehat{\Omega}_6^F$.

As regards crosstalk, preliminary simulations show that a residual crosstalk of -30 dB (as proposed for BIOMASS [18]) will yield rms FR errors of 0.07° for $\widehat{\Omega}_3^F$ and 0.02° for $\widehat{\Omega}_6^F$ when $\delta_i = -30$ dB, $i = 1{-}4$.

V. CONCLUSION

A set of FR estimators can be constructed from the imaginary parts of the off-diagonal terms in the measured covariance matrix of a distributed target. By combining these estimators with FR predictions based on GNSS TEC data, FR can be estimated without ambiguity, allowing unique correction of polarimetric data under arbitrarily large values of FR. Simulations indicate that $\widehat{\Omega}_3^F$ is the preferred estimator because it has the lowest sensitivity to both system noise and channel amplitude imbalance among all the estimators considered and has adequate tolerance to channel phase imbalance if calibration can reduce its residual values to around 1°.

Since no single FR estimator displays optimal resistance to all types of system effect, the likely system error budget after calibration will affect the choice of estimator, and better understanding of the estimators may allow us to combine the high tolerance to noise and channel amplitude imbalance of $\widehat{\Omega}_3^F$ with the overall system insensitivity of the Freeman estimator.

Further work will therefore include a more comprehensive theoretical analysis of the effects of system errors on the FR estimators, and development of an optimized procedure for correcting both FR and system errors, with a particular focus on the requirements and error budget of the BIOMASS mission.

REFERENCES

[1] W. B. Gail, "Effect of Faraday rotation on polarimetric SAR," *IEEE Trans. Aerosp. Electron. Syst.*, vol. 34, no. 1, pp. 301–308, Jan. 1998.

[2] F. Meyer, R. Bamler, N. Jakowski, and T. Fritz, "The potential of low-frequency SAR systems for mapping ionospheric TEC distributions," *IEEE Geosci. Remote Sens. Lett.*, vol. 3, no. 4, pp. 560–564, Oct. 2006.

[3] Z.-W. Xu, J. Wu, and Z.-S. Wu, "A survey of ionospheric effects on space-based radar," *Waves Random Media*, vol. 14, no. 12, pp. 189–272, Apr. 2004.

[4] A. Freeman and S. S. Saatchi, "On the detection of Faraday rotation in linearly polarized L-band SAR backscatter signatures," *IEEE Trans. Geosci. Remote Sens.*, vol. 42, no. 8, pp. 1607–1616, Aug. 2004.

[5] A. Freeman, "Calibration of linearly polarized polarimetric SAR data subject to Faraday rotation," *IEEE Trans. Geosci. Remote Sens.*, vol. 42, no. 8, pp. 1617–1624, Aug. 2004.

[6] A. Freeman, X.-Q. Pi, and B. Chapman, "Calibration of PalSAR polarimetric data," presented at the POLinSAR, Frascati, Italy, Jan., 2009.

[7] S. H. Bickel and R. H. T. Bates, "Effects of magneto-ionic propagation on the polarization scattering matrix," *Proc. IEEE*, vol. 53, no. 8, pp. 1089–1091, Aug. 1965.

[8] R.-Y. Qi and Y.-Q. Jin, "Analysis of the effects of Faraday rotation on spaceborne polarimetric SAR observations at P-band," *IEEE Trans. Geosci. Remote Sens.*, vol. 45, no. 5, pp. 1115–1122, May 2007.

[9] F. J. Meyer and J. B. Nicoll, "Prediction, detection, and correction of Faraday rotation in full-polarimetric L-band SAR data," *IEEE Trans. Geosci. Remote Sens.*, vol. 46, no. 10, pp. 3076–3086, Oct. 2008.

[10] M. Jehle, M. Rüegg, L. Zuberbühler, D. Small, and E. Meier, "Measurement of ionospheric Faraday rotation in simulated and real spaceborne SAR data," *IEEE Trans. Geosci. Remote Sens.*, vol. 46, no. 12, pp. 1162–1169, Dec. 2008.

[11] G. Sandberg, L. Eriksson, and L. Ulander, "Measurements of Faraday rotation using polarimetric PALSAR images," *IEEE Geosci. Remote Sens. Lett.*, vol. 6, no. 1, pp. 142–146, Jan. 2009.

[12] P. A. Wright, S. Quegan, N. S. Wheadon, and C. D. Hall, "Faraday rotation effects on L-band spaceborne data," *IEEE Trans. Geosci. Remote Sens.*, vol. 41, no. 12, pp. 2735–2744, Dec. 2003.

[13] A. Freeman, "Response to 'Corrections to 'Calibration of linearly polarized polarimetric SAR data subject to Faraday rotation''," *IEEE Trans. Geosci. Remote Sens.*, vol. 46, no. 4, p. 1279, Apr. 2008.

[14] M. Sekido, T. Kondo, E. Kawai, and M. Imae, "Evaluation of GPS-based ionospheric TEC map by comparing with VLBI data," *Radio Sci.*, vol. 38, no. 4, pp. 8-1–8-22, Jul. 2003.

[15] L. Mandrake, B. Wilson, C. Wang, G. Hajj, A. Mannucci, and X. Pi, "A performance evaluation of the operational Jet Propulsion Laboratory/University of Southern California Global Assimilation Ionospheric Model (JPL/USC GAIM)," *J. Geophys. Res.*, vol. 110, no. A12, pp. A12 306-1–A12 306-10, Dec. 2005.

[16] H. Balzter, M. Davidson, T. Le Toan, P. Paillou, K. Papathaniassiou, S. Plummer, S. Quegan, F. Rocca, S. S. Saatchi, H. Shugart, H. Freeman, K.-H. Erb, S. Schaphoff, W. Lucht, and M. Davidson, "BIOMASS report for assessment," Eur. Space Agency, Paris, France, 2008.

[17] T. Le Toan, A. Beaudoin, J. Riom, and D. Guyon, "Relating forest biomass to SAR data," *IEEE Trans. Geosci. Remote Sens.*, vol. 30, no. 2, pp. 403–411, Mar. 1992.

[18] S.-K. Lee, F. Kugler, I. Hajnsek, and K. Papathanassiou, "Bandwidth effects in Pol-InSAR performance at P-band," presented at the POLinSAR, Frascati, Italy, Jan., 2009.